Neutral-Beam-Injection on Wendelstein 7-X: Beam transmission, shine through and effect of plasma current

N. Rust[1], O. P. Ford[1], D. Hartmann[1], B. Heinemann[2], P. McNeely[1], R. Schroeder[1], A. Spanier[1], S. Äkäslomplo[1], R. C. Wolf[1], and the Wendelstein 7-X team[1]

[1]*Max-Planck-Institut für Plasmaphysik, Teilinstitut Greifswald, D-17491 Greifswald, Germany*

[2]*Max-Planck-Institut für Plasmaphysik, D-85748 Garching, Germany*

Abstract: This work presents details of the Wendelstein W7-X stellarator Neutral-Beam-Injector (NBI) system, and its effect on the beam dump, duct, heating efficiency and plasma current. During the last operation phase of the stellarator W7-X, the first of two NBI injectors (NI21) was taken into operation. It was equipped with two hydrogen sources with a neutral power before the duct of 2×1.7MW and a maximum pulse-length of 5s. Each injector is currently equipped with two ion sources. One source of NI21 was installed at a location optimized for maximum port transmission and another source at a location for maximum heating efficiency. The predictions for the heat load on the port liner and the beam dump are compared with the experimental findings for operating NI21 into the empty torus and into W7-X plasmas. In addition, the effects of NI operation on the overall plasma current are assessed.

1. Introduction: W7-X is equipped with two Neutral-Beam Injector (NBI)-Boxes (NI20 and NI21) for balanced injection. They are replicas of the ASDEX-Upgrade NBI-system [2] and each of them can to be equipped with up to 4 PINI-sized [3] RF ion sources [4] of 2.5MW (D^0, 60kV) or 1.7MW (H^0, 55kV) neutral power per source and a maximum pulse-length of 10s. For the last W7-X experimental campaign one of the two Injector boxes (NI21) was in operation with two 2 ion sources (source 7 and 8) operating in hydrogen. These are tangential source 8 and radial source 7 neutral beam sources with different physical characteristics. With only Box NI21 in operation no balanced injection is possible. Due to their position and the duct geometry the duct transmission and neutral power load to the duct protection is different for source 7 and 8 [5].

2. Transmission through the duct: The superconducting coils of the W7-X stellarator limit the size and shape of the duct. There are two constrictions caused by the planar and nonplanar W7-X coils near the duct. Detailed calculations of the beam transmission and the power load to the graphite elements mounted on a cooled CuCrZr duct protection and the optimization of the shape of the duct protection have been presented in [5]. In addition, design and optimization of the torus interface have been presented in [6]. The overall calculated duct transmission for source 7 is 91% and for source 8 is 84%. The tangential source suffers more from the duct constrictions. The limited transmission, especially for the more tangential source 8, leads to a power load to the duct protection. Calculations were made for hydrogen injection at 55keV assuming 1° divergence using the in-house code DesnB [7].

Fig. 1 shows the comparison of the calculated power load to the duct protection with the visible and near IR light observed with a borescope camera in the NBI-duct for source 7 (fig. 1a) and source 8 (fig. 1b). The elements of the duct that are heated are visible as bright areas in the camera picture. The brightest spot in the center is the location where the beam hits the beam dump area on the W7-X inner vessel opposite of the NBI port. The small spots left (source 7, 8) and right of the beam dump area (source 8) are reflections of the beam dump on the sidewall of the duct. As the borescope camera is located in the lower part of the duct, the glowing of the duct protection is visible left and right of the halo produced by beam-residual gas interaction. The more radial source 7, less affected by the port constrictions, has a power load to the duct that is significantly smaller (less than 0.5MW/m²) compared to source 8 (up to 2MW/m²). For source 7 the observed light on the left side of the duct shows the two faintly visible interaction areas predicted by the calculations. The duct protection on the right side of the duct shows nearly no glowing. Either the overall power load is too low to heat up the carbon protection up to a level of visible glowing, or it could be that source 7 is slightly shifted to the left. For source 8 as predicted no power load is visible on the left side, while the right side the carbon protections is glowing bright in the central part of the duct protection. For both sources there is a good agreement with the DensB calculations. This suggests that the optimization of the shape of the duct protection [5] works. For the entirely of the W7-X campaign, there was no single event of beam blocking due to additional neutral background gas released by a high power load on the duct surface.

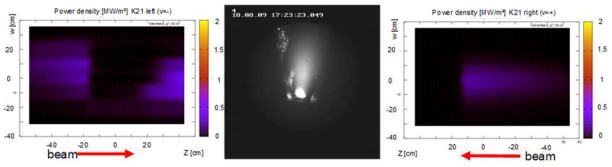

Fig.1a W7-X NBI power-load to the duct protection NI21 source 7 (hydrogen 55kV, 1° divergence): left side of the duct, observation visible and near IR light, right side of the duct (color scale 2MW/m²)

Fig.1b W7-X NBI power-load to the duct protection NI21 source 8 (hydrogen 55kV, 1° divergence): left side of the duct, observation visible and near IR light, right side of the duct (color scale 2MW/m²)

3. Shine through / heating profile: The prediction of the shine through presented in [5] for hydrogen injection (55kV) into a central density of 1.3E20/m^{-3} was 7% for source 7 and 4.5% for source 8. The basis of the old calculations was an assumed density profile. For more realistic calculations of both the shine through and the heating profile of source 7 and source 8 the W7-X plasma pulse 20181009.024 (high mirror configuration) with a pure NBI-plasma heating phase (1s-5s) alternating source 7 and source 8 was evaluated. For this evaluation profiles from the W7-X topical group “Profiles” and an equilibrium based on VMEC code calculations were used. All calculations were carried out with the ASCOT code [8] (Fig. 2).

Using the plasma with parameters given in Fig. 2, the global power distribution shown in table 1 was derived by the ASCOT code. The calculations for source 7 refer to 3.9s, the calculations for source 8 for refer to 4.9s. As already mentioned, the more radial source 7 has a better transmission through the

duct compared to source 8. On the other hand, both the shine through and the fast-ion-loss are larger for source 7 compared to source 8. In total the heating power for the more tangential source 8 is slightly higher compared to the more radial source 7.

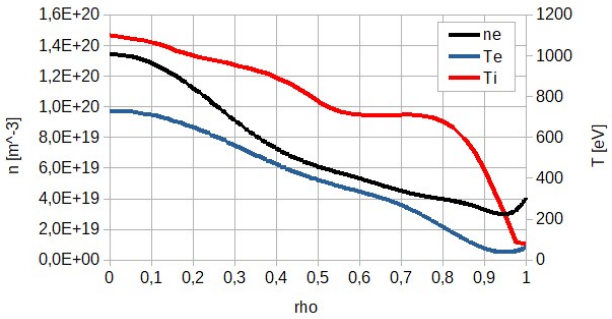

Fig.2a W7-X pulse 20181009.024: electron density, electron temperature, ion temperature

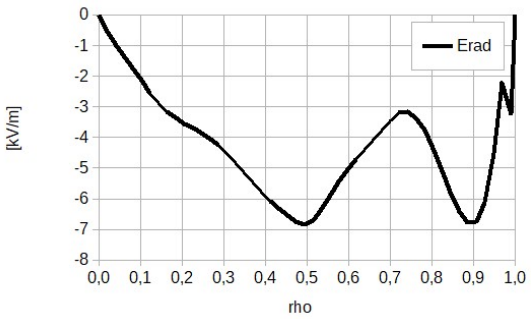

Fig.2b W7-X pulse 20181009.024: radial electric field

Fig. 3 shows the calculated heating profile for source 7 (Fig. 3a) and for source 8 (Fig. 3b). Although the source geometry is different, not only is the total heating power similar for both sources, but the heating power profile is nearly indistinguishable; at least, for this evaluated plasma pulse.

	Source 7	Source 8
power to vessel	1.87MW	1.69MW
shine through	0.13MW (6.7%)	0.08MW (4.0%)
fast-ion-loss	0.43MW	0.20MW
heating power	1.31MW	1.40MW

Table 1: Global distribution of the total NBI heating power. power to vessel, shine through, fast-ion-loss, total heating power

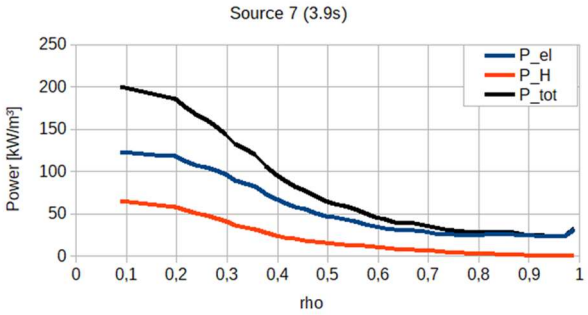

Fig.3a W7-X pulse 20181009.024: source 7 heating profile (electrons: blue, hydrogen ions: red, total: black)

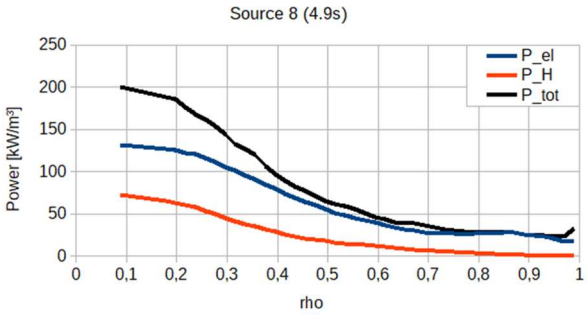

Fig.3b W7-X pulse 20181009.024: source 8 heating profile (electrons: blue, hydrogen ions: red, total: black)

4. NBI current drive: With only the NBI-box NI21 in operation balanced injection was impossible. The NBI driven current of one injector could not be compensated by the equivalent sources of the second injector, as described in [9]. The direction of the current drive of NI21 is negative, and therefore as predicted in [9] opposite to the bootstrap current; possibly not compensating the bootstrap current profile, but at least reducing its effect on the iota profile. The measured toroidal current in the pure

ECRH-phase of discharge 20181009.024 between 0s and 1s slightly positive, while during the following pure NBI phase after 1s, the toroidal current is negative.

For calculation of the NBI driven current ASCOT runs for the pure NBI phase of W7-X discharge 20181009.024 were performed for source 7 and source 8 (Fig.4). Although the heating power profile was nearly indistinguishable, the calculated toroidal NBI driven current is significant different for the more radial source 7 compared to the more tangential source 8. This must be related to the different source geometry. The absolute asymptotic value of the toroidal NBI driven current is -0.6kA for source 7 and -2.0kA for source 8.

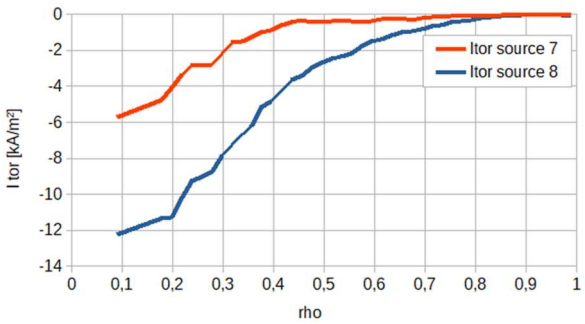

Fig.4 W7-X pulse 20181009.024: source 7 (red) and source 8 (blue) toroidal current drive profile

5. Conclusion: During the last W7-X campaign (OP1.2b) the NBI-injector NI21 with 2 sources, the more radial source 7 and the more tangential source 8, was operated using hydrogen at 55kV. The duct transmission is limited by some constrictions with the W7-X coils, especially for the more tangential source 8. The duct was observed using a visible light and near IR camera. The observed glowing of the graphite duct protection is in good agreement with simulations. Using observed plasma profile data, the shine through and the fast-ion-loss was calculated. From the results of that calculations it was found that these values are smaller for the more tangential source 8. Although the heating power profile for source 7 and 8 are similar, source 8 has a slightly higher heating power. The lower transmission is slightly overcompensated for by the combination of lower shine through and fast-ion-losses. For the NBI driven toroidal current there is a significant difference between the more radial source 7 and the more tangential source 8. The direction of the current drive of NI21 is negative and therefore opposite to the bootstrap current; possibly not compensating the bootstrap current profile, but at least reducing its effect on the iota profile.

Acknowledgments: *This work has been carried out within the framework of the EUROfusion Consortium and has received funding from the Euratom research and training programme 2014-2018 and 2019-2020 under grant agreement number 633053. The views and opinions expressed herein do not necessarily reflect those of the European Commission.*

[1] T. Klinger et al., Nuclear Fusion 59 (2019) 112004 doi: 10.1088/1741-4326/ab03a7

[2] A. Stäbler, J.-H. Feist, E. Speth, et al., Fusion Technology (1988) 620

[3] G. Duesing, H. Altmann, H. Falter, et al., Fusion Technology 11 (1987) 163

[4] E. Speth, M. Ciric, J.H. Feist, et al. Fusion Engineering and Design 46 (1999) 383

[5] N. Rust, B. Heinemann. B. Mendelevitch, A. Peacock, M. Smirnow, Fusion Engineering and Design 86 (2011) 728

[6] R. Nocentini, et al., Fusion Engineering and Design 100 (2015) 453

[7] N. Rust, H. Greuner, B. Heinemann, M. Kick, R. Riedl, E. Speth, Soft 2004

[8] S. Äkäslompolo et al., 3RD European Conference on Plasma Diagnostics 2019, Lisbon (prepared for submission)

[9] M. Schmidt, Y. Turkin, A. Werner, 31st EPS Conference on Plasma Phys. 28G (2004) P-1.120